DOI: 10.1002/ejic.200900615

Lanthanopolyoxometalates as Building Blocks for Multiwavelength Photoluminescent Organic–Inorganic Hybrid Materials

Carlos M. Granadeiro,[a] Rute A. S. Ferreira,[b] Paula C. R. Soares-Santos,[a] Luís D. Carlos,[b] and Helena I. S. Nogueira*[a]

Keywords: Polyoxometalates / Lanthanides / Organic-inorganic hybrid composites / Luminescence

Organic–inorganic hybrid materials were prepared by combining lanthanide(III) substituted Wells–Dawson anions as inorganic building blocks and 3-hydroxypicolinate (picOH) as the organic ligand. The organic–inorganic hybrids obtained $K_n[Ln_x(\alpha_2\text{-}P_2M_{17}O_{61})(picOH)_7]\cdot yH_2O$ (M^{VI} = W and Ln^{III} = La, Ce, Sm, Eu, Tb, Er; or M^{VI} = Mo and Ln^{III} = Eu) were characterized by chemical analysis and spectroscopic methods such as FTIR and FT-Raman, ^{31}P and ^{13}C MAS NMR spectroscopy. Photoluminescence measurements on the prepared hybrid materials were performed showing the intra-$4f^N$ emission in the visible (Eu^{III}, Tb^{III} compounds) and in the near-infrared (Er^{III} compound) spectral regions, being, in all the cases, sensitized by both the picOH ligand and the polyoxometalate moiety. A maximum quantum yield value of 0.18 was found for $K_{11}[Eu_2(\alpha_2\text{-}P_2Mo_{17}O_{61})(picOH)_7]\cdot 10H_2O$.

Introduction

Lanthanopolyoxometalates (LnPOMs) have been the subject of many studies since they were first reported by Peacock and Weakley in 1971.[1] Their chemical and structural diversity led to the publication of a large variety of crystal structures involving all series of lanthanides coordinated to polyoxometalates (POMs) such as $[W_5O_{18}]^{6-}$ moieties,[2] lacunary forms of the Keggin anion,[3] the Preyssler anion[4] or the lacunary forms of the Wells–Dawson anion.[5] Lanthanide coordination to a specific POM anion may lead to different positional isomers and to different stoichiometries, depending on the experimental conditions and on the lanthanide ion size.[6] The lanthanide ions may also act as linkers for the construction of POM chain structures[7] and 2D or 3D networks.[8]

The presence of the lanthanide confers specific functionalities to LnPOM compounds, in particular the photoluminescent properties.[9] We have been working on the preparation of new photoluminescent POM materials based on LnPOMs incorporated into layer double hydroxides,[10] assembled in layer-by-layer[11] and Langmuir–Blodget[12] thin films or encapsulated in core–shell silica nanoparticles. Detailed photoluminescence studies have shown that there is efficient emission from the LnPOMs in those materials, in particular for EuPOMs, with excitation paths that involve POM-to-europium charge-transfer transitions resulting from the interaction between the europium ion and the POM involving LMCT (ligand-to-metal charge-transfer) states associated with $O \rightarrow Eu$ and $O \rightarrow W$ transitions.[9] The introduction of a specific organic ligand into LnPOMs leads to distinct photoluminescent properties from the starting LnPOM as a result of an additional energy transfer mechanism originated in the organic ligand that may act as an antenna, transferring energy to the lanthanide ion. The latter effect has been observed by us in organic–inorganic hybrids containing LnPOMs and 3-hydroxypicolinic acid (HpicOH).[13,14] The sensitization of europium(III) luminescence by the 3-hydroxypicolinate ligand (picOH) was previously shown for the $[Eu(H_2O)(picOH)_2(\mu\text{-}HpicO)]\cdot 3H_2O$ complex, also used as a photoactive centre in nanocomposite materials with silica nanoparticles.[15]

Sensitization of europium(III) luminescence by both the picOH ligand and the POM moiety was observed in polynuclear tungsten and molybdenum(VI) complexes with picOH and europium(III) $[M_4O_{12}Eu(picOH)_3]$ (M^{VI} = W, Mo).[13] Our studies on organic–inorganic hybrid materials using $[Ln(W_5O_{18})_2]^{n-}$-type lanthanopolyoxoanions as building blocks and picOH as the organic ligand have also shown that lanthanide luminescence may be sensitized by both the ligand and the POM.[14] Preliminary luminescence experiments on the interaction of the $[Eu(H_2O)_3(\alpha_2\text{-}P_2W_{17}O_{61})(Eu_2(H_2O)_7)]^{44-}$ cluster with a set of organic ligands capable of sensitizing the luminescence of the europium(III) have been recently reported by Francesconi.[16]

Here we report the preparation of new organic–inorganic hybrid materials by using lanthanide(III)-substituted Wells–Dawson anions as inorganic building blocks and picOH as the organic ligand. The organic–inorganic hybrids obtained

[a] Department of Chemistry, CICECO, University of Aveiro, 3810-193 Aveiro, Portugal
Fax: +351-234370084
E-mail: helenanogueira@ua.pt
[b] Department of Physics, CICECO, University of Aveiro, 3810-193 Aveiro, Portugal

$K_n[Ln_x(\alpha_2\text{-}P_2M_{17}O_{61})(picOH)_7]\cdot yH_2O$ [M^{VI} = W and Ln^{III} = La (**1**), Ce (**2**), Sm (**3**), Eu (**4**), Tb (**6**), Er (**7**); or M^{VI} = Mo and Ln^{III} = Eu (**5**)] were characterized by chemical analysis and spectroscopic methods such as FTIR and FT-Raman, ^{31}P and ^{13}C MAS NMR spectroscopy. The corresponding isolated lanthanide(III) complexes of the α_2-isomer of the monolacunary Wells–Dawson anion $K_7[Ln(\alpha_2\text{-}P_2M_{17}O_{61})]\cdot xH_2O$ (abbreviated LnP_2M_{17}, where M^{VI} = W and Ln^{III} = La, Ce, Sm, Eu, Tb, Er; or M^{VI} = Mo and Ln^{III} = Eu) were also prepared for comparison purposes. Photoluminescence measurements on the prepared materials were performed to study the energy transfer processes by both the picOH ligand and the POM moiety.

Results and Discussion

Table 1 presents infrared and Raman spectroscopic data for the Wells–Dawson-derived LnPOM hybrids with 3-hydroxypicolinate **1**–**7** prepared in this work and for the related LnP_2W_{17} (prepared by literature procedures). The assignments of the picOH carboxylate asymmetric $\nu_{as}(CO_2)$ and symmetric $\nu_s(CO_2)$ stretches were based on those found in the literature for picOH complexes.[17] For hybrid compounds **1**–**7** the shifts of around 25 cm^{-1} observed in $\nu_{as}(CO_2)$, when compared with the corresponding HpicOH IR band at 1654 cm^{-1}, indicates that the ligand picOH in the hybrids is possibly coordinated to the lanthanide through a carboxylate oxygen atom. Regarding the inorganic moiety, the infrared and Raman spectra of the hybrid materials (Figure 1c shows Eu^{III} compound **4**) exhibit typical bands of the α_2-isomer of the Wells–Dawson anion, similar to those observed for LnP_2W_{17} (Figure 1b shows EuP_2W_{17}). The prepared plenary Wells–Dawson anion $[\alpha\text{-}P_2W_{18}O_{62}]^{6-}$ exhibits typical P–O stretches ν(P–O) at 1090 and 1020 cm^{-1} in the infrared spectrum (Figure 1a), whereas the P–O vibrations of the corresponding α_2-lacunary compound $[\alpha_2\text{-}P_2W_{17}O_{61}]^{7-}$ are located at 1082, 1051 and 1015 cm^{-1} (Table 1) according to the literature data.[18] Both hybrid materials **1**–**7** and the respective LnP_2W_{17} (Table 1) present a pattern similar to the latter compound for the IR bands assigned to ν(P–O). The metal-terminal oxygen stretches, ν(M=O), and the bridging metal–oxygen stretches, ν(M–O–M), of both hybrid materials **1**–**7** and respective LnP_2W_{17} are also found at comparable wavenumbers in the infrared and Raman spectra (Table 1).

The ^{31}P MAS NMR spectroscopic data for the solid LnP_2W_{17} (Ln^{III} = La, Sm, Eu) and corresponding picOH hybrids (**1**, **3** and **4**, respectively) are shown in Table 2. The two different sets of peaks in the NMR spectra clearly indicate the presence of the two phosphorus atoms from the Wells–Dawson structure (Figure 2). The ^{31}P MAS data of

Table 1. Infrared and Raman data (cm^{-1}) for the Wells–Dawson derived LnPOMs and the respective 3-hydroxypicolinate compounds.[a]

Compound	$\nu_{as}(CO_2)$	$\nu_s(CO_2)$	ν(P–O)	ν(W=O)	ν(W–O–W)
$K_8Na_3[La_2(\alpha_2\text{-}P_2W_{17}O_{61})(picOH)_7]\cdot 20H_2O$ (**1**)	1629 (vs)	1324 (m)	1083 (s), 1054 (m), 1020 (m)	941 (vs)	885 (s), 825 (vs), 786 (vs)
	1647 (m)	*1325 (w)*	*1057 (s), 1017 (vw)*	*975 (vs)*	*876 (m), 827 (s)*
$K_8Na_3[Ce_2(\alpha_2\text{-}P_2W_{17}O_{61})(picOH)_7]\cdot 20H_2O$ (**2**)	1631 (vs)	1324 (m)	1085 (s), 1056 (m), 1018 (m)	941 (vs)	885 (vs), 823 (vs), 773 (vs)
	1648 (m)	*1325 (w)*	*1058 (s), 1021 (vw)*	*968 (vs)*	*875 (m), 829 (s)*
$K_9Na_2[Sm_2(\alpha_2\text{-}P_2W_{17}O_{61})(picOH)_7]\cdot 25H_2O$ (**3**)	1625 (s)	1332 (m)	1083 (s), 1056 (m), 1024 (m)	939 (s)	889 (m), 829 (s), 777 (vs)
		1344 (w)	*1061 (m), 1053 (w)*	*975 (vs).*	*873 (m), 831 (m)*
$K_{11}[Eu_2(\alpha_2\text{-}P_2W_{17}O_{61})(picOH)_7]\cdot 20H_2O$ (**4**)	1627 (s)	1332 (m)	1083 (s), 1056 (m), 1024 (m)	941 (vs)	887 (s), 829 (vs), 771 (vs)
	1623 (vw)	*1343 (w)*	*1060 (w), 1018 (w)*	*977 (vs)*	*877 (m), 832 (m)*
$K_{11}[Eu_2(\alpha_2\text{-}P_2Mo_{17}O_{61})(picOH)_7]\cdot 10H_2O$ (**5**)	1640 (s)	1347 (s)	1048 (m), 1024 (m)	929 (vs)	892 (m), 826 (w), 799 (m)
	1648 (w)	*1344 (w)*	*1057 (m)*	*927 (vs)*	*894 (s), 836 (m)*
$K_{11}[Tb_2(\alpha_2\text{-}P_2W_{17}O_{61})(picOH)_7]\cdot 20H_2O$ (**6**)	1625 (vs)	1334 (m)	1083 (s), 1056 (m), 1025 (m)	941 (vs)	889 (s), 829 (vs), 777 (vs).
	1625 (vw)	*1345 (m)*	*1062 (s), 1012 (vw)*	*967 (s)*	*925 (m), 834 (m)*
$K_{14}[Er(\alpha_2\text{-}P_2W_{17}O_{61})(picOH)_7]\cdot 20H_2O$ (**7**)	1627 (s)	1336 (m)	1083 (s), 1056 (w), 1027 (w)	941 (vs)	890 (s), 829 (vs), 779 (vs)
	1620 (vw)	*1348 (m)*	*1063 (m), 1016 (w)*	*966 (sh.)*	*888 (m), 836 (m)*
$K_7[La(\alpha_2\text{-}P_2W_{17}O_{61})]\cdot 22H_2O$			1083 (s), 1054 (m), 1018 (m)	941 (vs)	885 (s), 819 (vs), 784 (vs)
			1017 (vw)	*976 (vs)*	*884 (m), 809 (vw)*
$K_7[Ce(\alpha_2\text{-}P_2W_{17}O_{61})]\cdot 22H_2O$			1079 (s), 1052 (m), 1018 (w)	933 (s)	881 (s), 808 (vs), 763 (vs)
			1018 (vw)	*975 (vs)*	*875 (m), 825 (sh.)*
$K_7[Sm(\alpha_2\text{-}P_2W_{17}O_{61})]\cdot 18H_2O$			1083 (s), 1056 (m), 1018 (m)	941 (vs)	889 (m), 816 (sh.), 777 (vs)
			1021 (w)	*976 (vs)*	*891 (m), 825 (vw)*
$K_7[Eu(\alpha_2\text{-}P_2W_{17}O_{61})]\cdot 18H_2O$			1085 (vs), 1056 (m), 1024 (m)	942 (vs)	890 (s), 816 (sh.), 779 (vs)
			1023 (w)	*967 (vs)*	*882 (m), 768 (vs)*
$K_7[Eu(\alpha_2\text{-}P_2Mo_{17}O_{61})]\cdot 8H_2O$			1080 (sh.), 1051 (s), 1022 (m)	937 (vs)	860 (s), 784 (sh.), 728 (vs)
				947 (m)	*867 (m), 810 (w)*
$K_7[Tb(\alpha_2\text{-}P_2W_{17}O_{61})]\cdot 18H_2O$			1083 (vs), 1056 (m), 1022 (m)	941 (vs)	890 (sh.), 819 (vs), 779 (vs)
			1019 (w)	*966 (s)*	*890 (m), 826 (w)*
$K_7[Er(\alpha_2\text{-}P_2W_{17}O_{61})]\cdot 20H_2O$			1085 (vs), 1056 (m), 1016 (m)	943 (vs)	889 (sh.), 805 (vs), 779 (vs)
			1024 (w)	*966 (vs)*	*891 (m), 803 (m)*
$K_{10}[\alpha_2\text{-}P_2W_{17}O_{61}]\cdot 20H_2O$			1082 (s), 1051 (m), 1015 (m)	940 (vs)	887 (s), 809 (vs), 737 (vs)
			1015 (w)	*967 (vs)*	*888 (m), 800 (w)*
$K_6[\alpha\text{-}P_2W_{18}O_{62}]\cdot 14H_2O$			1090 (s), 1020 (sh.)	959 (s)	912 (s), 781 (vs)
			1019 (w)	*971 (s)*	*923 (m), 860 (w)*

[a] Raman data in italics; v: very, s: strong, m: medium, w: weak, sh.: shoulder.

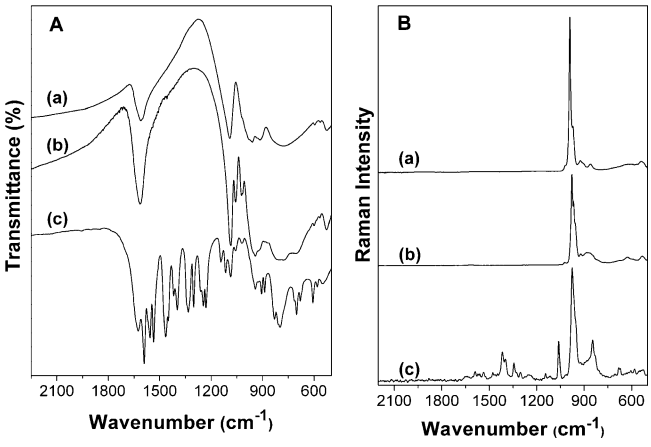

Figure 1. Infrared (A) and FT-Raman (B) spectra of (a) the plenary Wells–Dawson anion in $K_6[\alpha\text{-}P_2W_{18}O_{62}]\cdot 14H_2O$, (b) the respective europium(III) α_2-lacunary complex EuP_2W_{17} and (c) the hybrid compound $K_{11}[Eu_2(\alpha_2\text{-}P_2W_{17}O_{61})(picOH)_7]\cdot 20H_2O$ (**4**).

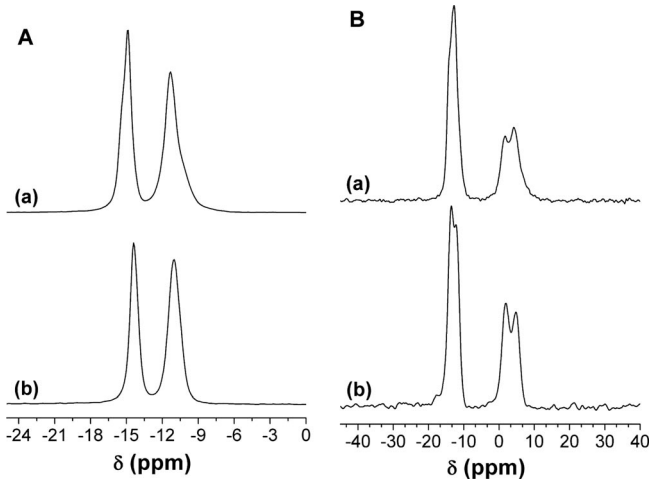

Figure 2. ^{31}P MAS NMR spectra of the samarium (A) and europium (B) Wells–Dawson derived LnPOMs LnP_2W_{17} (a) and the respective 3-hydroxypicolinate compounds **3** and **4** (b).

the europium compounds show peak splitting to two signal sets that can be due to a known disorder of the POM framework in the solids.[5] Nevertheless, the ^{31}P resonance values for the hybrids indicates the retention of the POM structure.

Table 2. ^{31}P MAS NMR spectroscopic data for the Wells–Dawson derived LnPOMs and the respective 3-hydroxypicolinate compounds (P1 is assigned to the phosphorus atom closer to the lanthanide coordination site and P2 to the one more distant[19]).

Compound	δ (ppm)	
	P1	P2
$K_{10}[\alpha_2\text{-}P_2W_{17}O_{61}]\cdot 20H_2O$	–6.7	–14.1
$K_7[La(\alpha_2\text{-}P_2W_{17}O_{61})]\cdot 22H_2O$	–7.8	–14.0
$K_8Na_3[La_2(\alpha_2\text{-}P_2W_{17}O_{61})(picOH)_7]\cdot 20H_2O$ (**1**)	–7.9	–14.2
$K_7[Sm(\alpha_2\text{-}P_2W_{17}O_{61})]\cdot 18H_2O$	–11.3	–14.9
$K_9Na_2[Sm_2(\alpha_2\text{-}P_2W_{17}O_{61})(picOH)_7]\cdot 25H_2O$ (**3**)	–11.0	–14.4
$K_7[Eu(\alpha_2\text{-}P_2W_{17}O_{61})]\cdot 18H_2O$	4.0	–13.0
	1.8	
$K_{11}[Eu_2(\alpha_2\text{-}P_2W_{17}O_{61})(picOH)_7]\cdot 20H_2O$ (**4**)	5.0	–12.2
	1.7	–13.6

The ^{13}C CPMAS NMR spectroscopic data for the solid picOH hybrids **1** and **3** (see Scheme 1 for carbon labelling and Table 3 for tentative assignments) confirms the presence of the picOH ligands in the hybrid materials, showing peak shifts from the free ligand. The shift of the C7 carbon atom supports a carboxylate coordination of the picOH ligands as suggested by the vibrational spectra.

Digital photographs under 366 nm radiation of EuP_2W_{17} (Figure 3a) and TbP_2W_{17} (identical to Figure 3a) and the respective picOH compounds $K_{11}[Eu_2(\alpha_2\text{-}P_2W_{17}O_{61})(picOH)_7]\cdot 20H_2O$ (**4**; Figure 3b) and $K_{11}[Tb_2(\alpha_2\text{-}P_2W_{17}O_{61})(picOH)_7]\cdot 20H_2O$ (**6**; Figure 3c) show that the emission properties of the compounds change in the organic–inorganic hybrid materials, when compared to the Wells–Dawson-derived LnPOMs. Photoluminescence measurements on the prepared materials were performed to study the presence of ligands-to-Ln^{3+} energy-transfer processes.

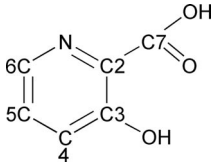

Scheme 1.

Figure 4 compares the excitation spectra of the Eu^{3+} α_2-lacunary polyoxotungstate (abbreviated EuP_2W_{17}) and polyoxomolybdate (abbreviated to EuP_2Mo_{17}) monitored within the $^5D_0 \rightarrow {}^7F_2$ transition. Both spectra display a series of intra-$4f^6$ lines ascribed to transitions between the $^7F_{0,1}$ ground states and the $^5D_{4-1}$, $^5G_{2-6}$ and $^5L_6$ excited levels. A low intensity broad band is also observed for EuP_2W_{17} (240–320 nm) and EuP_2Mo_{17} (280–330 nm). The excitation spectrum of the Tb^{3+} α_2-lacunary polyoxotungstate (abbreviated to TbP_2W_{17}) was monitored within the $^5D_4 \rightarrow {}^7F_5$ transition. The spectrum displays the intra-$4f^8$ $^7F_6 \rightarrow {}^5D_{3,2}$, $^5L_{10}$ (320–380 nm) and $^7F_6 \rightarrow {}^5D_4$ (488 nm) transitions and a broad band, already detected in the excitation spectrum of EuP_2W_{17} below 330 nm. The large broad bands detected in the UV region of all the compounds have also been observed in other materials containing W^{6+} or Mo^{6+} ions, being attributed to the presence of ligand-to-metal charge-transfer (LMCT) transitions resulting from the interaction between the lanthanide (Eu^{3+}, Tb^{3+}) ions and the POM moieties, namely, LMCT states associated with $O \rightarrow Eu/Tb$, $O \rightarrow W$ and $O \rightarrow Mo$ transitions.[11,12,20–27] In the case of TbP_2W_{17}, the contribution of the spin-forbidden (low-spin, LS, and high-spin, HS) interconfigurational fd transitions, discerned in the 250–310 nm region cannot be neglected.[28] The higher relative intensity of the Eu^{3+} and Tb^{3+} straight lines indicate that the metal ions are essentially excited through direct excitation into the intra-$4f^6$ (Eu^{3+}) and intra-$4f^8$ (Tb^{3+}) levels rather than by efficient intramolecular energy transfer involving the LMCT states.

Table 3. ^{13}C CPMAS NMR spectroscopic data for the 3-hydroxypicolinate hybrid compounds.

Compound	δ (ppm)					
	C2	C3	C4	C5	C6	C7
HpicOH	136	158	122	128	133	181
$K_8Na_3[La_2(\alpha_2\text{-}P_2W_{17}O_{61})(picOH)_7]\cdot 20H_2O$ (**1**)	140	159	128	128	131	175
$K_9Na_2[Sm_2(\alpha_2\text{-}P_2W_{17}O_{61})(picOH)_7]\cdot 25H_2O$ (**3**)	135	153	125	125	131	172
	140					177

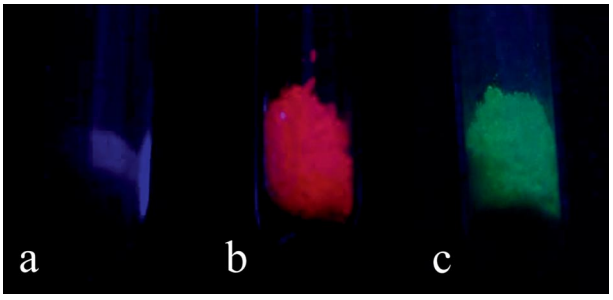

Figure 3. Digital photographs of (a) EuP_2W_{17} and the hybrid materials (b) $K_{11}[Eu_2(\alpha_2\text{-}P_2W_{17}O_{61})(picOH)_7]\cdot 20H_2O$ (**4**) and (c) $K_{11}[Tb_2(\alpha_2\text{-}P_2W_{17}O_{61})(picOH)_7]\cdot 20H_2O$ (**6**) under 366 nm radiation [the blue shadow in (a) is due to reflection of the UV light].

The excitation spectra of the hybrid materials containing picOH are displayed in Figure 4B. For the Eu^{3+}-based materials the spectra are formed of a large broad band with three main components at 255, 320 and 368 nm and of a series of intra-$4f^6$ lines, namely, between the $^7F_{0,1}$ and the $^5L_6$, $^5D_{2,1}$ levels. For the Tb^{3+} compound a similar broad band is also detected, being observed only a blueshift of the high wavelength component (from 368 to 350 nm) and the presence of the intra-$4f^8$ $^7F_6 \rightarrow {}^5D_4$ transition. The broad band can be mainly ascribed to transitions involving the $\pi\pi^*$ states of the chelate ring of the organic ligand.[13–15] The higher relative intensity of the ligand excited states with respect to that of the intra-4f lines (principally for **5** and **6**) points out that for the hybrid material the lanthanide sensitization process is the more efficient excitation path.

Figure 5 shows the emission spectra of the LnP_2M_{17} compounds excited under UV radiation. The spectra are composed of a series of straight lines ascribed to the Eu^{3+} $^5D_0 \rightarrow {}^7F_{0\text{–}4}$ transitions for EuP_2W_{17} and EuP_2Mo_{17} and assigned to the Tb^{3+} $^5D_4 \rightarrow {}^7F_{6\text{–}0}$ transitions for TbP_2W_{17}. Varying the excitation wavelength along the excitation spectra in Figure 4A, no significant changes are detected in the energy, full-width at half maximum (fwhm) and in the number of Stark components, pointing out that all the lanthanide ions occupy the same average local environment within each LnP_2M_{17} compound. Focusing on the Eu^{3+}-based POMs, the Eu^{3+} local environment is characterized by a low symmetry group without an inversion centre, as the higher relative intensity of the $^5D_0 \rightarrow {}^7F_2$ transition indicates. Further evidence of a single local Eu^{3+} local environment is given by the presence of a single line for the nondegenerated $^5D_0 \rightarrow {}^7F_0$ transition, whose energy (E_{00}) and fwhm ($fwhm_{00}$) values were estimated by fitting a single Gaussian function to the data in Figure 5A. The E_{00} and $fwhm_{00}$ values are, respectively, 17239.2 ± 0.1 cm^{-1} and

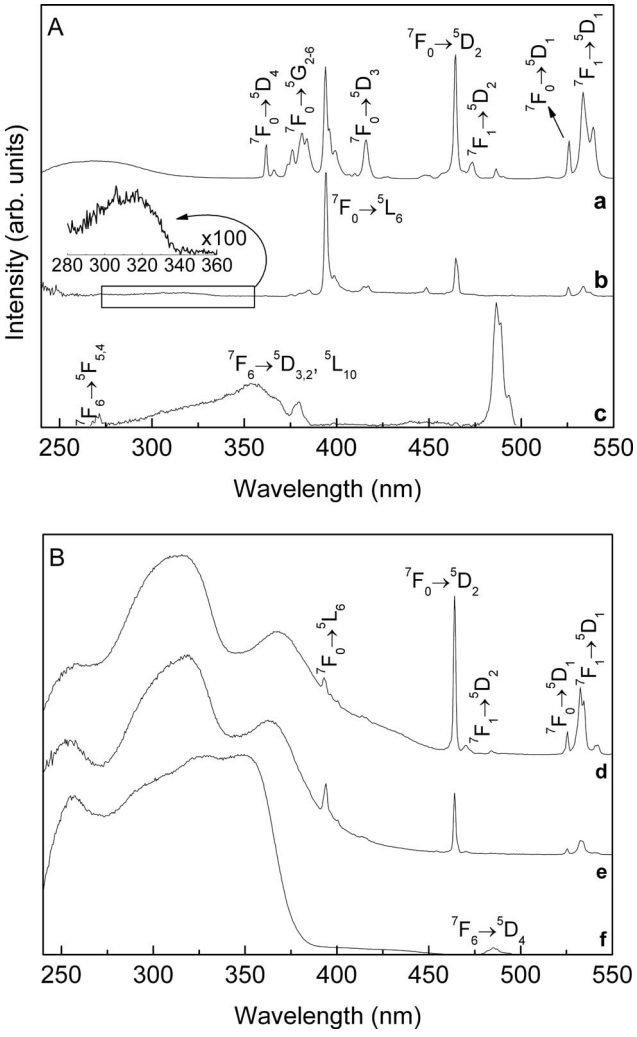

Figure 4. Room-temperature excitation spectra of (A) EuP_2W_{17} (a), EuP_2Mo_{17} (b) and TbP_2W_{17} (c) and of the (B) corresponding hybrid materials $K_{11}[Eu_2(\alpha_2\text{-}P_2W_{17}O_{61})(picOH)_7]\cdot 20H_2O$ **4** (d), $K_{11}[Eu_2(\alpha_2\text{-}P_2Mo_{17}O_{61})(picOH)_7]\cdot 10H_2O$ **5** (e) and $K_{11}[Tb_2(\alpha_2\text{-}P_2W_{17}O_{61})(picOH)_7]\cdot 20H_2O$ **6** (f). The monitoring wavelength was 612 and 544 nm for the Eu^{3+}- and Tb^{3+}-based materials, respectively.

24.9 ± 0.1 cm^{-1} for EuP_2W_{17} and 17242.7 ± 0.9 cm^{-1} and 48.5 ± 3.5 cm^{-1} for EuP_2Mo_{17}. The larger $fwhm_{00}$ value found for the latter POM relative to that determined for compound EuP_2W_{17} points out a larger distribution of Eu^{3+} local environments in the presence of Mo. Moreover, the different E_{00} values, number and relative intensity of Stark components readily point out that the Eu^{3+} first coordination sphere is different in both compounds.

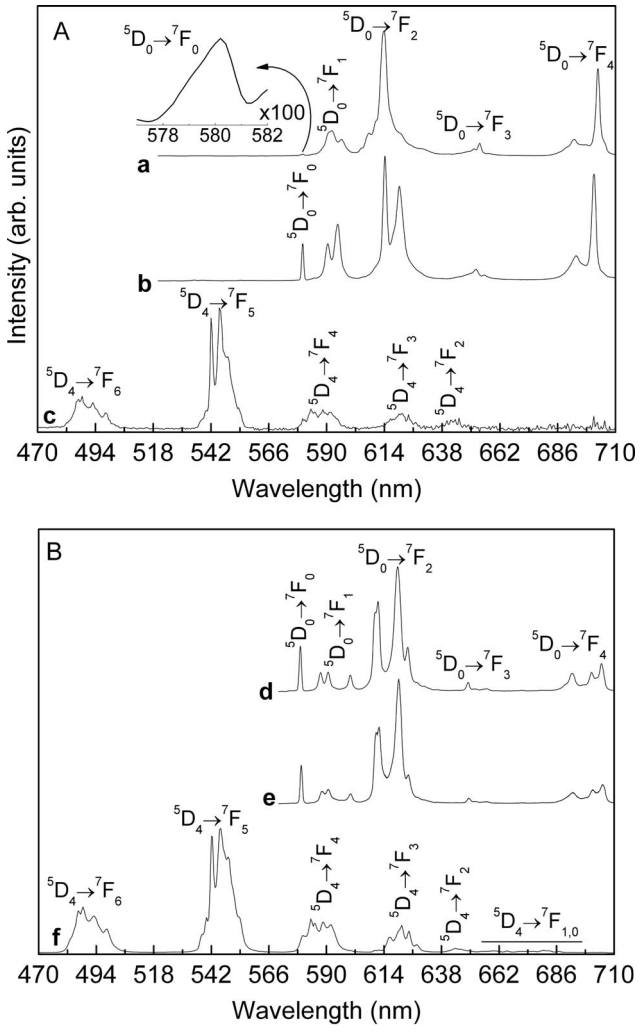

Figure 5. Room-temperature emission spectra of (A) EuP_2W_{17} (a) and EuP_2Mo_{17} (b) excited at 395 nm, and of TbP_2W_{17} (c) excited at 320 nm; and that of the (B) corresponding hybrid materials $K_{11}[Eu_2(\alpha_2\text{-}P_2W_{17}O_{61})(picOH)_7]\cdot 20H_2O$ **4** (d), $K_{11}[Eu_2(\alpha_2\text{-}P_2Mo_{17}O_{61})(picOH)_7]\cdot 10H_2O$ **5** (e) and $K_{11}[Tb_2(\alpha_2\text{-}P_2W_{17}O_{61})(picOH)_7]\cdot 20H_2O$ **6** (f).

Figure 5B displays the emission spectra of the hybrid materials containing picOH. Similarly to that found for the LnP_2M_{17} compounds, the emission spectra are formed of the Eu^{3+} $^5D_0 \rightarrow {}^7F_{0-4}$ transitions for **4** and **5** and assigned to the Tb^{3+} $^5D_4 \rightarrow {}^7F_{6-2}$ transitions in the case of **6**. All the spectra are independent of the excitation wavelength (300–465 nm), indicating a single distribution of local environments for the lanthanide ions within each hybrid material, similarly to that found for the POMs. The nonobservation of emission arising from the picOH ligands points out the existence of energy transfer between the organic ligand excited states and the Eu^{3+} intra-4f^6 and the Tb^{3+} intra-4f^8 levels, as the picOH ligand is known to emit at room temperature.[15]

The emission features of $K_{11}[Eu_2(\alpha_2\text{-}P_2W_{17}O_{61})(picOH)_7]\cdot 20H_2O$ (**4**) and $K_{11}[Eu_2(\alpha_2\text{-}P_2Mo_{17}O_{61})(picOH)_7]\cdot 10H_2O$ (**5**) were analysed in greater detail; in particular, the E_{00} and $fwhm_{00}$ values were estimated by using a single Gaussian function yielding to 17256.0 ± 0.1 cm^{-1} and 26.8 ± 0.1 cm^{-1}, respectively, for **4** and 17267.9 ± 0.1 cm^{-1} and 27.4 ± 0.2 cm^{-1}, respectively, for **5**. The difference in the E_{00} values indicates that the Eu^{3+} first coordination sphere is different within each hybrid. Comparing these features with those of the isolated POMs (namely, EuP_2W_{17} and EuP_2Mo_{17}) a blueshift in the E_{00} values is observed, whereas the E_{00} value previously reported for the isolated Eu^{3+}-derived picOH complex (17251.4 ± 0.1 cm^{-1})[15] is redshifted. The previous observations are in accordance with the fact that the Eu^{3+} local environment in the hybrids should involve both the picOH and POM ligands, besides water molecules.

In order to further quantify the different photoluminescence features of the POMs and of the respective hybrid materials, the lifetime values of the $^5D_0$ (Eu^{3+}) and $^5D_4$ (Tb^{3+}) excited states were estimated on the basis of the emission decay curves monitored within the more intense Eu^{3+} ($^5D_0 \rightarrow {}^7F_2$) and Tb^{3+} ($^5D_4 \rightarrow {}^7F_5$) transitions, respectively, and under direct intra-4f^6 ($^5D_2$, 465 nm) and intra-4f^8 ($^5D_3$, 350 nm) excitation. All the curves reveal a single exponential behaviour (not shown), which corroborates that all the lanthanide ions occupy the same average local environment within each compound. For the Eu^{3+}-containing materials, the obtained lifetime values are gathered in Table 4. For the Tb^{3+}-containing materials, an increase in the $^5D_4$ lifetime from 0.233 ± 0.005 ms in TbP_2W_{17} to 0.424 ± 0.002 ms was observed after the inclusion of the organic ligand in hybrid **6**.

Table 4. Lifetime (τ, ms), quantum efficiency (η), radiative, (k_r, ms^{-1}) and nonradiative, (k_{nr}, ms^{-1}), transition probabilities of the $^5D_0$ level and number of water molecules coordinated to the Eu^{3+} ion (n_w) for EuP_2W_{17}, EuP_2Mo_{17} and the correspondent hybrid compounds **4** and **5**. The parameters were estimated by using room-temperature spectra and excitation wavelength of 465 nm. The absolute emission quantum yield (ϕ) is also presented for the same excitation wavelength. The values in parentheses were acquired under 320 nm excitation wavelength.

	EuP_2W_{17}	EuP_2Mo_{17}	**4**	**5**
τ	0.525 ± 0.005	0.433 ± 0.002	0.377 ± 0.004	0.536 ± 0.003
k_r	0.272	0.494	0.455	0.592
k_{nr}	1.633	1.816	2.198	1.274
η	0.14	0.21	0.17	0.32
ϕ	0.01	0.18	n.m.[a]	0.04
			(0.04)	(0.08)
n_w	1.4 ± 0.1	1.6 ± 0.1	2.1 ± 0.1	1.0 ± 0.1

[a] Not measurable (<0.01).

The emission quantum yield was measured for all the materials by using direct intra-4f excitation and, for the hybrids, excited state excitation of the organic ligands. The maximum quantum yield value was measured for EuP_2Mo_{17} under intra-4f^6 excitation (Table 4). The measured values for hybrid **4** (smaller than that of the precursor compound) are similar to those found for SiO_2-poly(ethylene glycol) and SiO_2-glycidoxypropyltrimethoxysilane systems with $K_{13}[Eu(SiMo_xW_{11-x}O_{39})_2]$ (0.031–0.034).[29] Although the quantum yield values of TbP_2W_{17} lie below the

detection limits of our equipment (0.01), the presence of HpicOH moieties in hybrid **6** leads to an enhancement in the quantum yield values to 0.08 (320–350 nm excitation wavelength).

In order to further quantify the emission features of Eu^{3+}-containing materials, the radiative (k_r) and nonradiative (k_{nr}) transition probabilities of the $^5D_0$ level and the quantum efficiency (η), $\eta = k_r/(k_r + k_{nr})$ were estimated by using a procedure based on the room-temperature emission spectrum and $^5D_0$ lifetime values.[26] The radiative contribution may be calculated from the relative intensities of the $^5D_0 \rightarrow {}^7F_{0-4}$ transitions (the $^5D_0 \rightarrow {}^7F_{5,6}$ branching ratios are neglected due to their poor relative intensity with respect to that of the remaining $^5D_0 \rightarrow {}^7F_{0-4}$ lines). The $^5D_0 \rightarrow {}^7F_1$ transition does not depend on the local ligand field and thus may be used as a reference for the whole spectrum, in vacuo $A_{0-1} = 14.65\ s^{-1}$.[27] An effective refractive index of 1.5 was used leading to $A(^5D_0 \rightarrow {}^7F_1) \approx 50\ s^{-1}$. The values found for η, k_r and k_{nr} are gathered in Table 4. Comparing the η values of the EuP_2M_{17} materials with those previously reported for a polyoxotungstoeuropate,[14] the values in Table 4 are smaller. In spite of higher k_r values, EuP_2W_{17} and EuP_2Mo_{17} display much higher k_{nr} values relative to those known for the polyoxotungstoeuropate, namely, k_r and k_{nr} values of 0.153 and 0.326 cm^{-1} for $[Eu(PW_{11}O_{39})_2]^{11-}$ and 0.139 and 0.215 cm^{-1} for $[EuW_{10}O_{36}]^{9-}$.[14]

Comparing the LnP_2M_{17} compounds and the hybrid materials, an increase in the η values is observed. For the case of compounds EuP_2Mo_{17} and **5**, such an increase is due to both an increase in the k_r value and a decrease in the k_{nr} value. For EuP_2W_{17} and **4**, after incorporation of the organic ligand, although an increase in the radiative transition probability k_r around 40% is observed, there is a higher increase (70%) in the nonradiative transition probability, k_{nr}. On the basis of these results, we may presume that the decrease in the absolute emission quantum yield of the Eu^{3+} materials after inclusion of the ligands is due to the intrinsic nonradiative paths associated with the 3-hydroxypicolinic, despite the presence of ligand-to-Eu^{3+} energy transfer.

Moreover, the variations in the η and A_{nr} values may be rationalized in terms of the number of water molecules coordinated to the Eu^{3+} ions (n_w) based on the empirical formula $n_w = 1.11 \times (\tau^{-1} - k_r - 0.31)$.[26,30] The results obtained for EuP_2M_{17} indicate 1.5 water molecules, in average, in the first Eu^{3+} coordination sphere. The 1:1 $Ln[\alpha_2\text{-}P_2W_{17}O_{61}]^{10-}$ species are described as dimers in the solid state.[31] In the crystal structure[31] of $K_{13}(H_3O)[Eu(H_2O)_3(\alpha_2\text{-}P_2W_{17}O_{61})]_2 \cdot 2KCl \cdot 50H_2O$, the Eu atom is bound to the four oxygen atoms in the cap vacancy of the heteropolyanion, to a terminal tungsten oxygen atom and to three water molecules. The number of 1.5 water molecules coordinated to Eu^{3+} obtained by us for EuP_2W_{17} is inferior, possibly due to the fact that our solids were obtained as powders, under a different crystallization procedure. The presence of HpicOH moieties lead to an increase in the number of water molecules belonging to the Eu^{3+} first coordination shell in EuP_2W_{17}; the opposite result is observed for **5** (Table 4). The different n_w values indicate different Eu^{3+} first coordination spheres in **4** and **5**, as mentioned above.

Organic–inorganic hybrids emitting in the near-infrared (NIR) spectral region were prepared by combining Er^{3+}-substituted Wells–Dawson anions and picOH ligands. Figure 6 shows the excitation spectrum monitored in the NIR spectral region for the $K_{14}[Er(\alpha_2\text{-}P_2W_{17}O_{61})(picOH)_7] \cdot 20H_2O$ (**7**) hybrid. The spectrum displays a large broad band attributed to the ligands excited states and a series of Er^{3+} transitions. Similarly to that found for the Eu^{3+} and Tb^{3+} hybrid analogous (Figure 4), the Er^{3+} ions are sensitized by the ligands. Under UV excitation through the ligands excited states, the emission spectrum displays the Er^{3+} transition.

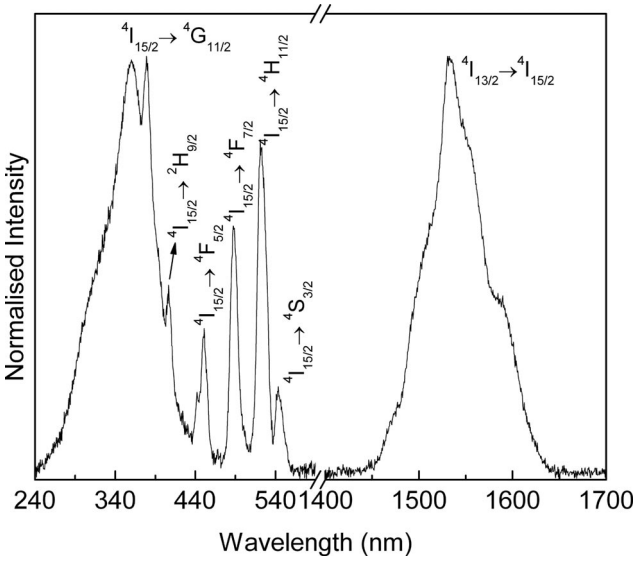

Figure 6. Room-temperature NIR emission (1400–1700 nm) and UV/Vis excitation (240–560 nm) spectra of the $K_{14}[Er(\alpha_2\text{-}P_2W_{17}O_{61})(picOH)_7] \cdot 20H_2O$ (**7**) hybrid excited at 360 nm and monitored at 1535 nm, respectively.

Conclusions

In this work we were able to synthesize new organic–inorganic hybrid materials composed of lanthanide(III)-substituted Wells–Dawson anions as inorganic building blocks and 3-hydroxypicolinate as the organic ligand. The hybrids are multiwavelength emitters from the UV/Vis to the NIR spectral regions. The intra-4f emission of the Eu^{3+}, Tb^{3+} and Er^{3+} ions is sensitized by the 3-hydroxypicolinate ligand and the POM moiety. The incorporation of the 3-hydroxypicolinate ligand induces an enhancement in the $^5D_0$ quantum efficiency (from 0.14 to 0.17 and 0.21 to 0.32 for the W and Mo containing materials, respectively), whereas a decrease in the quantum yield value (e.g., 0.18 to 0.04 for the Mo containing materials) was observed.

Experimental Section

General: All reagents were obtained from Aldrich and used without further purification. The Wells–Dawson polyoxotungstate was pre-

pared according to the method described by Nadjo,[32] whereas its α_2-lacunary compound was prepared by the method of Contant.[33] The α_2-lacunary polyoxomolybdate $K_{10}[\alpha_2\text{-}P_2M_{17}O_{61}]\cdot 20H_2O$ was synthesized by using a modified procedure from the method described by Román.[34]

Synthesis of $K_7[Ln(\alpha_2\text{-}P_2M_{17}O_{61})]\cdot xH_2O$ (LnP_2M_{17}), where M^{VI} = W and Ln^{III} = La, Ce, Sm, Eu, Tb, Er; or M^{VI} = Mo and Ln^{III} = Eu: The α_2-lacunary LnPOMs were prepared by using a modified procedure based on the method described by Francesconi.[31] The α_2-lacunary salt $K_{10}[\alpha_2\text{-}P_2M_{17}O_{61}]\cdot 20H_2O$ (0.051 mmol) was dissolved in a 0.5 M aqueous solution of sodium acetate (3.0 mL, pH adjusted to 5.5) at 70 °C. A solution of the lanthanide chloride (0.15 mmol) in water (2 mL) was added dropwise to the previous solution followed by the addition of a solution of potassium chloride (1.50 g, 20.0 mmol) in water (10 mL). The resulting mixture was stirred at 70 °C for 30 min, after which it was placed in the refrigerator for 72 h with the formation of a colourless precipitate. The precipitate was filtered, washed with ethanol and dried in a desiccator over silica gel.

Synthesis of $K_n[Ln_x(\alpha_2\text{-}P_2M_{17}O_{61})(picOH)_7]\cdot yH_2O$, where M^{VI} = W and Ln^{III} = La (1), Ce (2), Sm (3), Eu (4), Tb (6), Er (7); or M^{VI} = Mo and Ln^{III} = Eu (5): The α_2-lacunary salt $K_{10}[\alpha_2\text{-}P_2M_{17}O_{61}]\cdot 20H_2O$ (0.051 mmol) was dissolved in a 0.5 M aqueous solution of sodium acetate (3.0 mL, pH adjusted to 5.5) at 70 °C. A solution of 3-hydroxypicolinic acid (98%, 0.087 g, 0.61 mmol) in water (10 mL) and a solution of the lanthanide chloride (0.15 mmol) in water (2 mL) were added dropwise to the previous stirring solution. Finally, a solution of potassium chloride (1.50 g, 20.0 mmol) in water (10 mL) was added to the resulting solution. The mixture was stirred at 70 °C for 30 min and placed in the refrigerator for 72 h with the formation of a light beige precipitate. The precipitate was filtered, washed with ethanol and dried in a desiccator over silica gel.

1: $K_8Na_3[La_2(\alpha_2\text{-}P_2W_{17}O_{61})(C_6H_4NO_3)_7]\cdot 20H_2O$ (6149.95): calcd. C 8.20, H 1.11, K 5.09, La 4.52, N 1.59, P 1.01, W 50.8; found C 8.90, H 1.36, K 5.20, La 4.73, N 1.58, P 1.07, W 49.9.

2: $K_8Na_3[Ce_2(\alpha_2\text{-}P_2W_{17}O_{61})(C_6H_4NO_3)_7]\cdot 20H_2O$ (6152.38): calcd. C 8.20, H 1.11, Ce 4.55, K 5.08, N 1.59, P 1.01, W 50.8; found C 9.04, H 1.12, Ce 5.93, K 5.42, N 1.77, P 1.06, W 47.4.

3: $K_9Na_2[Sm_2(\alpha_2\text{-}P_2W_{17}O_{61})(C_6H_4NO_3)_7]\cdot 25H_2O$ (6279.05): calcd. C 8.03, H 1.25, K 5.60, N 1.56, P 0.99, Sm 4.79, W 49.8; found C 8.30, H 1.41, K 5.68, N 1.55, P 0.94, Sm 4.42, W 47.1.

4: $K_{11}[Eu_2(\alpha_2\text{-}P_2W_{17}O_{61})(C_6H_4NO_3)_7]\cdot 20H_2O$ (6224.39): calcd. C 8.10, H 1.10, Eu 4.88, K 6.91, N 1.58, P 1.00, W 50.2; found C 8.34, H 1.34, Eu 4.66, K 6.36, N 1.59, P 0.92, W 48.4.

5: $K_{11}[Eu_2(\alpha_2\text{-}P_2Mo_{17}O_{61})(C_6H_4NO_3)_7]\cdot 10H_2O$ (4549.76): calcd. C 11.1, H 1.06, Eu 6.68, K 9.45, Mo 35.8, N 2.15, P 1.36; found C 14.0, H 0.95, Eu 4.39, K 10.6, Mo 30.5, N 2.88, P 0.40.

6: $K_{11}[Tb_2(\alpha_2\text{-}P_2W_{17}O_{61})(C_6H_4NO_3)_7]\cdot 20H_2O$ (6238.32): calcd. C 8.09, H 1.10, K 6.89, N 1.57, P 0.99, Tb 5.10, W 50.1; found C 7.40, H 1.13, K 9.00, N 1.41, P 0.90, Tb 5.33, W 42.2.

7: $K_{14}[Er(\alpha_2\text{-}P_2W_{17}O_{61})(C_6H_4NO_3)_7]\cdot 20H_2O$ (6205.02): calcd. C 8.13, H 1.10, Er 2.70, K 8.82, N 1.58, P 1.00, W 50.4; found C 7.37, H 1.09, Er 1.89, K 10.7, N 1.63, P 1.02, W 48.4.

Instrumentation: FTIR spectra were obtained with a Mattson 7000 spectrophotometer with the use of KBr pellets. FT-Raman spectra were recorded with a Bruker RFS100/S FT-Raman spectrophotometer (Nd:YAG laser, 1064 nm excitation). Elemental analyses were performed with a CHNS-932 elemental analyser (for carbon, nitrogen and hydrogen) at the Microanalysis Laboratory and by ICP-AES at the Central Laboratory for Analysis of the University of Aveiro. The ^{13}C CPMAS and ^{31}P MAS NMR spectra were recorded at 9.4 T with a Bruker Avance 400 WB spectrometer (DSX model) operating at 400.1 MHz by using 7 mm o.d. ZrO_2 rotors. The ^{13}C CPMAS spectra were recorded with 4 μs 90° pulses, spinning rate of 7 kHz and 3 s recycle delays. The ^{31}P MAS NMR were recorded with 2.5 μs 90° pulses, a spinning rate of 15 kHz and 60 s recycle delays. The photoluminescence in the near-infrared (NIR) and in the ultraviolet/visible (UV/Vis) spectral ranges were recorded between 12 K and room temperature with a modular double grating excitation spectrofluorimeter with a TRIAX 320 emission monochromator (Fluorolog-3, Jobin Yvon-Spex) coupled to a H9170–75 Hamamatsu photomultiplier and to a R928 Hamamatsu photomultiplier, respectively, using the front face and right angle mode. The excitation source was a 450 W Xe arc lamp. The emission spectra were corrected for detection and optical spectral response of the spectrofluorimeter and the excitation spectra monitored in the visible spectral range were corrected for the spectral distribution of the lamp intensity using a photodiode reference detector. The emission decay measurements were acquired between 14 K and room temperature with the setup described above by using a pulsed Xe-Hg lamp (6 μs pulse at half width and 20–30 μs tail). The absolute emission quantum yields were measured at room temperature using a Quantum Yield Measurement System C9920–02 from Hamamatsu (experimental error 10%) with a 150 W Xenon lamp coupled to a monochromator for wavelength discrimination, an integrating sphere as sample chamber and a multichannel analyzer for signal detection.

Acknowledgments

The authors would like to thank the Fundação para a Ciência e a Tecnologia (Portugal) for funding under the POCI 2010 and PTDC programs and FEDER (POCI/QUI/58887/2004 and PTDC/QUI/67712/2006) and for post graduation grants to C.M.G. (SFRH/BD/30137/2006) and P.C.R.S.S. (SFRH/BPD/14954/2004).

[1] R. D. Peacock, T. J. R. Weakley, *J. Chem. Soc. A* **1971**, 1836–1839.
[2] T. Yamase, T. Ozeki, M. Tosaka, *Acta Crystallogr., Sect. C* **1994**, *50*, 1849–1852.
[3] F. L. Sousa, F. A. Almeida Paz, A. M. V. Cavaleiro, J. Klinowski, H. I. S. Nogueira, *Chem. Commun.* **2004**, 2656–2657.
[4] D. Volkmer, A. Du Chesne, D. G. Kurth, H. Schnablegger, P. Lehmann, M. J. Koop, A. Müller, *J. Am. Chem. Soc.* **2000**, *122*, 1995–1998.
[5] W. Huang, M. Schopfer, C. Zhang, R. C. Howell, L. Todaro, B. A. Gee, L. C. Francesconi, T. Polenova, *J. Am. Chem. Soc.* **2008**, *130*, 481–490.
[6] C. Zhang, L. Bensaid, D. McGregor, X. Fang, R. C. Howell, B. Burton-Pye, Q. Luo, L. Todaro, L. C. Francesconi, *J. Cluster Sci.* **2006**, *17*, 389–425.
[7] M. Sadakane, M. H. Dickman, M. T. Pope, *Angew. Chem. Int. Ed.* **2000**, *39*, 2914–2916.
[8] P. Mialane, L. Lisnard, A. Mallard, J. Marrot, E. Antic-Fidancev, P. Aschehoug, D. Vivien, F. Secheresse, *Inorg. Chem.* **2003**, *42*, 2102–2108.
[9] T. Yamase, *Chem. Rev.* **1998**, *98*, 307–325.
[10] F. L. Sousa, M. Pillinger, R. A. Sá Ferreira, C. M. Granadeiro, A. M. V. Cavaleiro, J. Rocha, L. D. Carlos, T. Trindade, H. I. S. Nogueira, *Eur. J. Inorg. Chem.* **2006**, 726–734.
[11] F. L. Sousa, A. C. A. S. Ferreira, R. A. S. Ferreira, A. M. V. Cavaleiro, L. D. Carlos, H. I. S. Nogueira, J. Rocha, T. Trindade, *J. Nanosci. Nanotechnol.* **2004**, *4*, 214–220.

[12] F. L. Sousa, A. S. Ferreira, R. A. S. Ferreira, A. M. V. Cavaleiro, L. D. Carlos, H. I. S. Nogueira, T. Trindade, *J. Alloys Compd.* **2004**, *374*, 371–376.
[13] M. J. E. Rodrigues, F. A. A. Paz, R. A. S. Ferreira, L. D. Carlos, H. I. S. Nogueira, *Mater. Sci. Forum* **2006**, *514–516*, 1305–1312.
[14] C. M. Granadeiro, R. A. S. Ferreira, P. C. R. Soares-Santos, L. D. Carlos, H. I. S. Nogueira, *J. Alloys Compd.* **2008**, *451*, 422–425.
[15] P. C. R. Soares-Santos, H. I. S. Nogueira, V. Félix, M. G. B. Drew, R. A. S. Ferreira, L. D. Carlos, T. Trindade, *Chem. Mater.* **2003**, *15*, 100–108.
[16] C. Zhang, R. C. Howell, D. McGregor, L. Bensaid, S. Rahyab, M. Nayshtut, S. Lekperic, L. C. Francesconi, *C. R. Chim.* **2005**, *8*, 1035–1044.
[17] S. M. O. Quintal, H. I. S. Nogueira, H. M. Carapuça, V. Félix, M. G. B. Drew, *J. Chem. Soc., Dalton Trans.* **2001**, 3196–3201.
[18] F. Cavani, R. Mezzogori, A. Trovarelli, *J. Mol. Catal. A* **2003**, *204–205*, 599–607.
[19] J. Bartis, M. Dankova, J. J. Lessman, Q.-H. Luo, W. D. Horrocks, L. C. Francesconi, *Inorg. Chem.* **1999**, *38*, 1042–1053.
[20] a) T. Yamase, H. Naruke, *J. Chem. Soc., Dalton Trans.* **1991**, 285–292; b) T. Yamase, H. Naruke, *J. Phys. Chem. B* **1999**, *103*, 8850–8857.
[21] S. Neeraj, N. Kijima, A. K. Cheetham, *Chem. Phys. Lett.* **2004**, *387*, 2–6.
[22] T. Yamase, H. Naruke, *Coord. Chem. Rev.* **1991**, *111*, 83–90.
[23] M. Sugeta, T. Yamase, *Bull. Chem. Soc. Jpn.* **1993**, *66*, 444–449.
[24] R. Ballardini, Q. G. Mulazzani, M. Venturi, F. Bolletta, B. Balzani, *Inorg. Chem.* **1984**, *23*, 300–305.
[25] a) J. Wang, H. S. Wang, L. S. Fu, F. Y. Liu, H. J. Zhang, *Thin Solid Films* **2002**, *414*, 256–261; b) J. Wang, H. Wang, F. Liu, L. Fu, H. Zhang, *J. Lumin.* **2003**, *101*, 63–70; c) X. L. Wang, Y. H. Wang, C. W. Hu, E. B. Wang, *Mater. Lett.* **2002**, *56*, 305–311; d) J. Wang, H. Wang, L. Fu, F. Liu, H. Zhang, *Thin Solid Films* **2002**, *415*, 242–247.
[26] a) L. D. Carlos, Y. Messaddeq, H. F. Brito, R. A. S. Ferreira, V. D. Bermudez, S. J. L. Ribeiro, *Adv. Mater.* **2000**, *12*, 594–598; b) L. D. Carlos, R. A. S. Ferreira, V. D. Bermudez, S. J. L. Ribeiro, *Adv. Mater.* **2009**, *21*, 509–534.
[27] M. H. V. Werts, R. T. F. Jukes, J. W. Verhoeven, *Phys. Chem. Chem. Phys.* **2002**, *4*, 1542–1548.
[28] a) M. Laroche, J. L. Doualan, S. Girard, J. Margerie, R. J. Moncorgé, *J. Opt. Soc. Am. B* **2000**, *17*, 1291–1303; b) L. van Pierterson, M. F. Reid, G. W. Burdick, A. Meijerink, *Phys. Rev. B* **2002**, *65*, 045114/1.
[29] A. M. Klonkowski, B. Grobelna, S. But, S. Lis, *J. Non-Cryst. Solids* **2006**, *352*, 2213–2219.
[30] R. M. Supkowski, W. D. W. Horrocks Jr., *Inorg. Chim. Acta* **2002**, *340*, 44–48.
[31] Q. Luo, R. C. Howell, J. Bartis, M. Dankova, W. D. Horrocks, A. L. Rheingold, L. C. Francesconi, *Inorg. Chem.* **2002**, *41*, 6112–6117.
[32] I.-M. Mbomekalle, Y. W. Lu, B. Keita, L. Nadjo, *Inorg. Chem. Commun.* **2004**, *7*, 86–90.
[33] R. Contant, *Inorg. Synth.* **1990**, *27*, 104–111.
[34] A. S. J. Wéry, J. M. Gutiérrez-Zorrilla, A. Luque, M. Ugalde, P. Román, *Polyhedron* **1997**, *16*, 2589–2597.

Received: July 1, 2009
Published Online: October 29, 2009

